

Directional limits on persistent gravitational waves using LIGO S5 science data

J. Abadie²⁹, B. P. Abbott²⁹, R. Abbott²⁹, M. Abernathy⁶⁶, T. Accadia²⁷, F. Acernese^{19ac}, C. Adams³¹, R. Adhikari²⁹, P. Ajith²⁹, B. Allen^{2,78}, G. S. Allen⁵², E. Amador Ceron⁷⁸, R. S. Amin³⁴, S. B. Anderson²⁹, W. G. Anderson⁷⁸, F. Antonucci^{22a}, M. A. Arain⁶⁵, M. C. Araya²⁹, M. Aronsson²⁹, K. G. Arun²⁶, Y. Aso²⁹, S. M. Aston⁶⁴, P. Astone^{22a}, D. Atkinson³⁰, P. Aufmuth²⁸, C. Aubert², S. Babak¹, P. Baker³⁷, G. Ballardin¹³, S. Ballmer²⁹, D. Barker³⁰, S. Barnum³², F. Barone^{19ac}, B. Barr⁶⁶, P. Barriga⁷⁷, L. Barsotti³², M. Barsuglia⁴, M. A. Barton³⁰, I. Bartos¹², R. Bassiri⁶⁶, M. Bastarrika⁶⁶, J. Bauchrowitz², Th. S. Bauer^{41a}, B. Behnke¹, M.G. Beker^{41a}, A. Belletoile²⁷, M. Benacquista⁵⁹, A. Bertolini², J. Betzwieser²⁹, N. Beveridge⁶⁶, P. T. Beyersdorf⁴⁸, S. Bigotta^{21ab}, I. A. Bilenko³⁸, G. Billingsley²⁹, J. Birch³¹, S. Birindelli^{43a}, R. Biswas⁷⁸, M. Bitossi^{21a}, M. A. Bizouard^{26a}, E. Black²⁹, J. K. Blackburn²⁹, L. Blackburn³², D. Blair⁷⁷, B. Bland³⁰, M. Blom^{41a}, C. Boccara^{26b}, O. Bock², T. P. Bodiya³², R. Bondarescu⁵⁴, F. Bondu^{43b}, L. Bonelli^{21ab}, R. Bonnand³³, R. Bork²⁹, M. Born², S. Bose⁷⁹, L. Bosi^{20a}, B. Bouhou⁴, M. Boyle⁸, S. Braccini^{21a}, C. Bradaschia^{21a}, P. R. Brady⁷⁸, V. B. Braginsky³⁸, J. E. Brau⁷¹, J. Breyer², D. O. Bridges³¹, A. Brillet^{43a}, M. Brinkmann², V. Brisson^{26a}, M. Britzger², A. F. Brooks²⁹, D. A. Brown⁵³, R. Budzyński^{45b}, T. Bulik^{45cd}, H. J. Bulten^{41ab}, A. Buonanno⁶⁷, J. Burguet-Castell⁷⁸, O. Burmeister², D. Buskulic²⁷, C. Buy⁴, R. L. Byer⁵², L. Cadonati⁶⁸, G. Cagnoli^{17a}, J. Cain⁵⁶, E. Calloni^{19ab}, J. B. Camp³⁹, E. Campagna^{17ab}, P. Campsie⁶⁶, J. Cannizzo³⁹, K. Cannon²⁹, B. Canuel¹³, J. Cao⁶¹, C. Capano⁵³, F. Carbognani¹³, S. Caride⁶⁹, S. Caudill³⁴, M. Cavaglià⁵⁶, F. Cavalier^{26a}, R. Cavalieri¹³, G. Cella^{21a}, C. Cepeda²⁹, E. Cesarini^{17b}, T. Chalermongsak²⁹, E. Chalkley⁶⁶, P. Charlton¹¹, E. Chassande-Mottin⁴, S. Chelkowski⁶⁴, Y. Chen⁸, A. Chincarini¹⁸, N. Christensen¹⁰, S. S. Y. Chua⁵, C. T. Y. Chung⁵⁵, D. Clark⁵², J. Clark⁹, J. H. Clayton⁷⁸, F. Cleva^{43a}, E. Coccia^{23ab}, C. N. Colacino^{21ab}, J. Colas¹³, A. Colla^{22ab}, M. Colombini^{22b}, R. Conte⁷³, D. Cook³⁰, T. R. Corbitt³², N. Cornish³⁷, A. Corsi^{22a}, C. A. Costa³⁴, J.-P. Coulon^{43a}, D. M. Coward⁷⁷, D. C. Coyne²⁹, J. D. E. Creighton⁷⁸, T. D. Creighton⁵⁹, A. M. Cruise⁶⁴, R. M. Culter⁶⁴, A. Cumming⁶⁶, L. Cunningham⁶⁶, E. Cuoco¹³, K. Dahl², S. L. Danilishin³⁸, R. Dannenberg²⁹, S. D'Antonio^{23a}, K. Danzmann^{2,28}, K. Das⁶⁵, V. Dattilo¹³, B. Daudert²⁹, M. Davier^{26a}, G. Davies⁹, A. Davis¹⁴, E. J. Daw⁵⁷, R. Day¹³, T. Dayanga⁷⁹, R. De Rosa^{19ab}, D. DeBra⁵², J. Degallaix², M. del Prete^{21ac}, V. Dergachev²⁹, R. DeRosa³⁴, R. DeSalvo²⁹, P. Devanka⁹, S. Dhurandhar²⁵, L. Di Fiore^{19a}, A. Di Lieto^{21ab}, I. Di Palma², M. Di Paolo Emilio^{23ac}, A. Di Virgilio^{21a}, M. Díaz⁵⁹, A. Dietz²⁷, F. Donovan³², K. L. Dooley⁶⁵, E. E. Doomes⁵¹, S. Dorsher⁷⁰, E. S. D. Douglas³⁰, M. Drago^{44cd}, R. W. P. Drever⁶, J. C. Driggers²⁹, J. Dueck², J.-C. Dumas⁷⁷, T. Eberle², M. Edgar⁶⁶, M. Edwards⁹, A. Effler³⁴, P. Ehrens²⁹, R. Engel²⁹, T. Etzel²⁹, M. Evans³², T. Evans³¹, V. Fafone^{23ab}, S. Fairhurst⁹, Y. Fan⁷⁷, B. F. Farr⁴², D. Fazi⁴², H. Fehrmann², D. Feldbaum⁶⁵, I. Ferrante^{21ab}, F. Fiducaro^{21ab}, L. S. Finn⁵⁴, I. Fiori¹³, R. Flaminio³³, M. Flanigan³⁰, K. Flasch⁷⁸, S. Foley³², C. Forrest⁷², E. Forsi³¹, N. Fotopoulos⁷⁸, J.-D. Fournier^{43a}, J. Franc³³, S. Frasca^{22ab}, F. Frasconi^{21a}, M. Frede², M. Frei⁵⁸, Z. Frei¹⁵, A. Freise⁶⁴, R. Frey⁷¹, T. T. Fricke³⁴, D. Friedrich², P. Fritschel³², V. V. Frolov³¹, P. Fulda⁶⁴, M. Fyffe³¹, M. Galimberti³³, L. Gammaitoni^{20ab}, J. A. Garofoli⁵³, F. Garufi^{19ab}, G. Gemme¹⁸, E. Genin¹³, A. Gennai^{21a}, I. Gholami¹, S. Ghosh⁷⁹, J. A. Giaime^{34,31}, S. Giampanis², K. D. Giardino³¹, A. Giazotto^{21a}, C. Gill⁶⁶, E. Goetz⁶⁹, L. M. Goggin⁷⁸, G. González³⁴, M. L. Gorodetsky³⁸, S. Gößler², R. Gouaty²⁷, C. Graef², M. Granata⁴, A. Grant⁶⁶, S. Gras⁷⁷, C. Gray³⁰, R. J. S. Greenhalgh⁴⁷, A. M. Gretarsson¹⁴, C. Greverie^{43a}, R. Grosso⁵⁹, H. Grote², S. Grunewald¹, G. M. Guidi^{17ab}, E. K. Gustafson²⁹, R. Gustafson⁶⁹, B. Hage²⁸, P. Hall⁹, J. M. Hallam⁶⁴, D. Hammer⁷⁸, G. Hammond⁶⁶, J. Hanks³⁰, C. Hanna²⁹, J. Hanson³¹, J. Harms⁶, G. M. Harry³², I. W. Harry⁹, E. D. Harstad⁷¹, K. Haughian⁶⁶, K. Hayama⁴⁰, J.-F. Hayau^{43b}, T. Hayler⁴⁷, J. Heefner²⁹, H. Heitmann⁴³, P. Hello^{26a}, I. S. Heng⁶⁶, A. W. Heptonstall²⁹, M. Hewitson², S. Hild⁶⁶, E. Hirose⁵³, D. Hoak⁶⁸, K. A. Hodge²⁹, K. Holt³¹, D. J. Hosken⁶³, J. Hough⁶⁶, E. J. Howell⁷⁷, D. Hoyland⁶⁴, D. Huet¹³, B. Hughey³², S. Husa⁶², S. H. Huttner⁶⁶, T. Huynh-Dinh³¹, D. R. Ingram³⁰, R. Inta⁵, T. Isogai¹⁰, A. Ivanov²⁹, P. Jaranowski^{45e}, W. W. Johnson³⁴, D. I. Jones⁷⁵, G. Jones⁹, R. Jones⁶⁶, L. Ju⁷⁷, P. Kalmus²⁹, V. Kalogera⁴², S. Kandhasamy⁷⁰, J. B. Kanner⁶⁷, E. Katsavounidis³², K. Kawabe³⁰, S. Kawamura⁴⁰, F. Kawazoe², W. Kells²⁹, D. G. Keppel²⁹, A. Khalaidovski², F. Y. Khalili³⁸, E. A. Khazanov²⁴, H. Kim², P. J. King²⁹, D. L. Kinzel³¹, J. S. Kissel³⁴, S. Klimenko⁶⁵, V. Kondrashov²⁹, R. Kopparapu⁵⁴, S. Koranda⁷⁸, I. Kowalska^{45c}, D. Kozak²⁹, T. Krause⁵⁸, V. Kringel², S. Krishnamurthy⁴², B. Krishnan¹, A. Królak^{45af}, G. Kuehn², J. Kullman², R. Kumar⁶⁶, P. Kwee²⁸, M. Landry³⁰, M. Lang⁵⁴, B. Lantz⁵², N. Lastzka², A. Lazzarini²⁹, P. Leaci¹, J. Leong², I. Leonor⁷¹, N. Leroy^{26a}, N. Letendre²⁷, J. Li⁵⁹, T. G. F. Li^{41a}, N. Liguori^{44ab}, H. Lin⁶⁵, P. E. Lindquist²⁹, N. A. Lockerbie⁷⁶, D. Lodhia⁶⁴, M. Lorenzini^{17a}, V. Lorette^{26b}, M. Lormand³¹, G. Losurdo^{17a}, P. Lu⁵², J. Luan⁸, M. Lubinski³⁰, A. Lucianetti⁶⁵, H. Lück^{2,28}, A. D. Lundgren⁵³, B. Machenschalk², M. MacInnis³², M. Mageswaran²⁹, K. Mailand²⁹, E. Majorana^{22a}, C. Mak²⁹, I. Maksimovic^{26b}, N. Man^{43a}, I. Mandel⁴², V. Mandic⁷⁰, M. Mantovani^{21ac}, F. Marchesoni^{20a},

F. Marion²⁷, S. Márka¹², Z. Márka¹², E. Maros²⁹, J. Marque¹³, F. Martelli^{17ab}, I. W. Martin⁶⁶, R. M. Martin⁶⁵, J. N. Marx²⁹, K. Mason³², A. Masserot²⁷, F. Matichard³², L. Matone¹², R. A. Matzner⁵⁸, N. Mavalvala³², R. McCarthy³⁰, D. E. McClelland⁵, S. C. McGuire⁵¹, G. McIntyre²⁹, G. McIvor⁵⁸, D. J. A. McKechnan⁹, G. Meadors⁶⁹, M. Mehmet², T. Meier²⁸, A. Melatos⁵⁵, A. C. Melissinos⁷², G. Mendell³⁰, D. F. Menéndez⁵⁴, R. A. Mercer⁷⁸, L. Merrill⁷⁷, S. Meshkov²⁹, C. Messenger², M. S. Meyer³¹, H. Miao⁷⁷, C. Michel³³, L. Milano^{19ab}, J. Miller⁶⁶, Y. Minenkov^{23a}, Y. Mino⁸, S. Mitra²⁹, V. P. Mitrofanov³⁸, G. Mitselmakher⁶⁵, R. Mittleman³², B. Moe⁷⁸, M. Mohan¹³, S. D. Mohanty⁵⁹, S. R. P. Mohapatra⁶⁸, D. Moraru³⁰, J. Moreau^{26b}, G. Moreno³⁰, N. Morgado³³, A. Morgia^{23ab}, T. Morioka⁴⁰, K. Mors², S. Mosca^{19ab}, V. Moscatelli^{22a}, K. Mossavi², B. Mours²⁷, C. M. Mow-Lowry⁵, G. Mueller⁶⁵, S. Mukherjee⁵⁹, A. Mullavey⁵, H. Müller-Ebhardt², J. Munch⁶³, P. G. Murray⁶⁶, T. Nash²⁹, R. Nawrodt⁶⁶, J. Nelson⁶⁶, I. Neri^{20ab}, G. Newton⁶⁶, A. Nishizawa⁴⁰, F. Nocera¹³, D. Nolting³¹, E. Ochsner⁶⁷, J. O'Dell⁴⁷, G. H. Oggin²⁹, R. G. Oldenburg⁷⁸, B. O'Reilly³¹, R. O'Shaughnessy⁵⁴, C. Osthelder²⁹, D. J. Ottaway⁶³, R. S. Ottens⁶⁵, H. Overmier³¹, B. J. Owen⁵⁴, A. Page⁶⁴, G. Pagliaroli^{23ac}, L. Palladino^{23ac}, C. Palomba^{22a}, Y. Pan⁶⁷, C. Pankow⁶⁵, F. Paoletti^{21a,13}, M. A. Papa^{1,78}, S. Pardi^{19ab}, M. Pareja², M. Parisi^{19b}, A. Pasqualetti¹³, R. Passaquieti^{21ab}, D. Passuello^{21a}, P. Patel²⁹, D. Pathak⁹, M. Pedraza²⁹, L. Pekowsky⁵³, S. Penn¹⁶, C. Peralta¹, A. Perreca⁶⁴, G. Persichetti^{19ab}, M. Pichot^{43a}, M. Pickenpack², F. Piergiovanni^{17ab}, M. Pietka^{45e}, L. Pinard³³, I. M. Pinto⁷⁴, M. Pitkin⁶⁶, H. J. Pletsch², M. V. Plissi⁶⁶, R. Poggiani^{21ab}, F. Postiglione⁷³, M. Prato¹⁸, V. Predoi⁹, L. R. Price⁷⁸, M. Prijatelj², M. Principe⁷⁴, R. Prix², G. A. Prodi^{44ab}, L. Prokhorov³⁸, O. Puncken², M. Punturo^{20a}, P. Puppato^{22a}, V. Quetschke⁵⁹, F. J. Raab³⁰, D. S. Rabeling^{41ab}, T. Radke¹, H. Radkins³⁰, P. Raffai¹⁵, M. Rakhmanov⁵⁹, B. Rankins⁵⁶, P. Rapagnani^{22ab}, V. Raymond⁴², V. Re^{44ab}, C. M. Reed³⁰, T. Reed³⁵, T. Regimbau^{43a}, S. Reid⁶⁶, D. H. Reitze⁶⁵, F. Ricci^{22ab}, R. Riesen³¹, K. Riles⁶⁹, P. Roberts³, N. A. Robertson^{29,66}, F. Robinet^{26a}, C. Robinson⁹, E. L. Robinson¹, A. Rocchi^{23a}, S. Roddy³¹, C. Röver², L. Rolland²⁷, J. Rollins¹², J. D. Romano⁵⁹, R. Romano^{19ac}, J. H. Romie³¹, D. Rosińska^{45g}, S. Rowan⁶⁶, A. Rüdiger², P. Ruggi¹³, K. Ryan³⁰, S. Sakata⁴⁰, M. Sakosky³⁰, F. Salemi², L. Sammut⁵⁵, L. Sancho de la Jordana⁶², V. Sandberg³⁰, V. Sannibale²⁹, L. Santamaría¹, G. Santostasi³⁶, S. Saraf⁴⁹, B. Sassolas³³, B. S. Sathyaprakash⁹, S. Sato⁴⁰, M. Satterthwaite⁵, P. R. Saulson⁵³, R. Savage³⁰, R. Schilling², R. Schnabel², R. M. S. Schofield⁷¹, B. Schulz², B. F. Schutz^{1,9}, P. Schwinberg³⁰, J. Scott⁶⁶, S. M. Scott⁵, A. C. Searle²⁹, F. Seifert²⁹, D. Sellers³¹, A. S. Sengupta²⁹, D. Sentenac¹³, A. Sergeev²⁴, D. A. Shaddock⁵, B. Shapiro³², P. Shawhan⁶⁷, D. H. Shoemaker³², A. Sibley³¹, X. Siemens⁷⁸, D. Sigg³⁰, A. Singer²⁹, A. M. Sintes⁶², G. Skelton⁷⁸, B. J. J. Slagmolen⁵, J. Slutsky³⁴, J. R. Smith⁷, M. R. Smith²⁹, N. D. Smith³², K. Somiya⁸, B. Sorazu⁶⁶, F. C. Speirits⁶⁶, L. Sperandio^{23ab}, A. J. Stein³², L. C. Stein³², S. Steinlechner², S. Steplewski⁷⁹, A. Stochino²⁹, R. Stone⁵⁹, K. A. Strain⁶⁶, S. Strigin³⁸, A. S. Stroerer³⁹, R. Sturani^{17ab}, A. L. Stuver³¹, T. Z. Summerscales³, M. Sung³⁴, S. Susmithan⁷⁷, P. J. Sutton⁹, B. Swinkels¹³, G. P. Szokoly¹⁵, D. Talukder⁷⁹, D. B. Tanner⁶⁵, S. P. Tarabrin², J. R. Taylor², R. Taylor²⁹, P. Thomas³⁰, K. A. Thorne³¹, K. S. Thorne⁸, E. Thrane^{70,a} and A. Thüring²⁸, C. Titsler⁵⁴, K. V. Tokmakov^{66,76}, A. Toncelli^{21ab}, M. Tonelli^{21ab}, O. Torre^{21ac}, C. Torres³¹, C. I. Torrie^{29,66}, E. Tournefier²⁷, F. Travasso^{20ab}, G. Traylor³¹, M. Trias⁶², J. Trummer²⁷, K. Tseng⁵², L. Turner²⁹, D. Ugolini⁶⁰, K. Urbanek⁵², H. Vahlbruch²⁸, B. Vaishnav⁵⁹, G. Vajente^{21ab}, M. Vallisneri⁸, J. F. J. van den Brand^{41ab}, C. Van Den Broeck⁹, S. van der Putten^{41a}, M. V. van der Sluys⁴², A. A. van Veggel⁶⁶, S. Vass²⁹, R. Vaulin⁷⁸, M. Vavoulidis^{26a}, A. Vecchio⁶⁴, G. Vedovato^{44c}, J. Veitch⁹, P. J. Veitch⁶³, C. Veltkamp², D. Verkindt²⁷, F. Vetrano^{17ab}, A. Viceré^{17ab}, A. E. Villar²⁹, J.-Y. Vinet^{43a}, H. Vocca^{20a}, C. Vorvick³⁰, S. P. Vyachanin³⁸, S. J. Waldman³², L. Wallace²⁹, A. Wanner², R. L. Ward²⁹, M. Was^{26a}, P. Wei⁵³, M. Weinert², A. J. Weinstein²⁹, R. Weiss³², L. Wen^{8,77}, S. Wen³⁴, P. Wessels², M. West⁵³, T. Westphal², K. Wette⁵, J. T. Whelan⁴⁶, S. E. Whitcomb²⁹, D. White⁵⁷, B. F. Whiting⁶⁵, C. Wilkinson³⁰, P. A. Willems²⁹, L. Williams⁶⁵, B. Willke^{2,28}, L. Winkelmann², W. Winkler², C. C. Wipf³², A. G. Wiseman⁷⁸, G. Woan⁶⁶, R. Wooley³¹, J. Worden³⁰, I. Yakushin³¹, H. Yamamoto²⁹, K. Yamamoto², D. Yeaton-Massey²⁹, S. Yoshida⁵⁰, P. Yu⁷⁸, M. Yvert²⁷, M. Zanolin¹⁴, L. Zhang²⁹, Z. Zhang⁷⁷, C. Zhao⁷⁷, N. Zotov³⁵, M. E. Zucker³², J. Zweizig²⁹

¹Albert-Einstein-Institut, Max-Planck-Institut für Gravitationsphysik, D-14476 Golm, Germany

²Albert-Einstein-Institut, Max-Planck-Institut für Gravitationsphysik, D-30167 Hannover, Germany

³Andrews University, Berrien Springs, MI 49104 USA

⁴Laboratoire AstroParticule et Cosmologie (APC) Université Paris Diderot, CNRS: IN2P3, CEA: DSM/IRFU, Observatoire de Paris 10, rue A.Domon et L.Duquet, 75013 Paris - France

⁵Australian National University, Canberra, 0200, Australia

⁶California Institute of Technology, Pasadena, CA 91125, USA

⁷California State University Fullerton, Fullerton CA 92831 USA

⁸Caltech-CaRT, Pasadena, CA 91125, USA

⁹Cardiff University, Cardiff, CF24 3AA, United Kingdom

- ¹⁰ Carleton College, Northfield, MN 55057, USA
- ¹¹ Charles Sturt University, Wagga Wagga, NSW 2678, Australia
- ¹² Columbia University, New York, NY 10027, USA
- ¹³ European Gravitational Observatory (EGO), I-56021 Cascina (PI), Italy
- ¹⁴ Embry-Riddle Aeronautical University, Prescott, AZ 86301 USA
- ¹⁵ Eötvös Loránd University, Budapest, 1117 Hungary
- ¹⁶ Hobart and William Smith Colleges, Geneva, NY 14456, USA
- ¹⁷ INFN, Sezione di Firenze, I-50019 Sesto Fiorentino^a; Università degli Studi di Urbino 'Carlo Bo', I-61029 Urbino^b, Italy
- ¹⁸ INFN, Sezione di Genova; I-16146 Genova, Italy
- ¹⁹ INFN, Sezione di Napoli^a; Università di Napoli 'Federico II'^b Complesso Universitario di Monte S. Angelo, I-80126 Napoli; Università di Salerno, Fisciano, I-84084 Salerno^c, Italy
- ²⁰ INFN, Sezione di Perugia^a; Università di Perugia^b, I-06123 Perugia, Italy
- ²¹ INFN, Sezione di Pisa^a; Università di Pisa^b; I-56127 Pisa; Università di Siena, I-53100 Siena^c, Italy
- ²² INFN, Sezione di Roma^a; Università 'La Sapienza'^b, I-00185 Roma, Italy
- ²³ INFN, Sezione di Roma Tor Vergata^a; Università di Roma Tor Vergata, I-00133 Roma^b; Università dell'Aquila, I-67100 L'Aquila^c, Italy
- ²⁴ Institute of Applied Physics, Nizhny Novgorod, 603950, Russia
- ²⁵ Inter-University Centre for Astronomy and Astrophysics, Pune - 411007, India
- ²⁶ LAL, Université Paris-Sud, IN2P3/CNRS, F-91898 Orsay^a; ESPCI, CNRS, F-75005 Paris^b, France
- ²⁷ Laboratoire d'Annecy-le-Vieux de Physique des Particules (LAPP), Université de Savoie, CNRS/IN2P3, F-74941 Annecy-Le-Vieux, France
- ²⁸ Leibniz Universität Hannover, D-30167 Hannover, Germany
- ²⁹ LIGO - California Institute of Technology, Pasadena, CA 91125, USA
- ³⁰ LIGO - Hanford Observatory, Richland, WA 99352, USA
- ³¹ LIGO - Livingston Observatory, Livingston, LA 70754, USA
- ³² LIGO - Massachusetts Institute of Technology, Cambridge, MA 02139, USA
- ³³ Laboratoire des Matériaux Avancés (LMA), IN2P3/CNRS, F-69622 Villeurbanne, Lyon, France
- ³⁴ Louisiana State University, Baton Rouge, LA 70803, USA
- ³⁵ Louisiana Tech University, Ruston, LA 71272, USA
- ³⁶ McNeese State University, Lake Charles, LA 70609 USA
- ³⁷ Montana State University, Bozeman, MT 59717, USA
- ³⁸ Moscow State University, Moscow, 119992, Russia
- ³⁹ NASA/Goddard Space Flight Center, Greenbelt, MD 20771, USA
- ⁴⁰ National Astronomical Observatory of Japan, Tokyo 181-8588, Japan
- ⁴¹ Nikhef, National Institute for Subatomic Physics, P.O. Box 41882, 1009 DB Amsterdam^a; VU University Amsterdam, De Boelelaan 1081, 1081 HV Amsterdam^b, The Netherlands
- ⁴² Northwestern University, Evanston, IL 60208, USA
- ⁴³ Université Nice-Sophia-Antipolis, CNRS, Observatoire de la Côte d'Azur, F-06304 Nice^a; Institut de Physique de Rennes, CNRS, Université de Rennes 1, 35042 Rennes^b, France
- ⁴⁴ INFN, Gruppo Collegato di Trento^a and Università di Trento^b, I-38050 Povo, Trento, Italy; INFN, Sezione di Padova^c and Università di Padova^d, I-35131 Padova, Italy
- ⁴⁵ IM-PAN 00-956 Warsaw^a; Warsaw University 00-681 Warsaw^b; Astronomical Observatory Warsaw University 00-478 Warsaw^c; CAMK-PAN 00-716 Warsaw^d; Białystok University 15-424 Białystok^e; IPJ 05-400 Świerk-Otwock^f; Institute of Astronomy 65-265 Zielona Góra^g, Poland
- ⁴⁶ Rochester Institute of Technology, Rochester, NY 14623, USA
- ⁴⁷ Rutherford Appleton Laboratory, HSIC, Chilton, Didcot, Oxon OX11 0QX United Kingdom
- ⁴⁸ San Jose State University, San Jose, CA 95192, USA
- ⁴⁹ Sonoma State University, Rohnert Park, CA 94928, USA
- ⁵⁰ Southeastern Louisiana University, Hammond, LA 70402, USA
- ⁵¹ Southern University and A&M College, Baton Rouge, LA 70813, USA
- ⁵² Stanford University, Stanford, CA 94305, USA
- ⁵³ Syracuse University, Syracuse, NY 13244, USA
- ⁵⁴ The Pennsylvania State University, University Park, PA 16802, USA
- ⁵⁵ The University of Melbourne, Parkville VIC 3010, Australia
- ⁵⁶ The University of Mississippi, University, MS 38677, USA
- ⁵⁷ The University of Sheffield, Sheffield S10 2TN, United Kingdom
- ⁵⁸ The University of Texas at Austin, Austin, TX 78712, USA
- ⁵⁹ The University of Texas at Brownsville and Texas Southmost College, Brownsville, TX 78520, USA
- ⁶⁰ Trinity University, San Antonio, TX 78212, USA
- ⁶¹ Tsinghua University, Beijing 100084 China
- ⁶² Universitat de les Illes Balears, E-07122 Palma de Mallorca, Spain
- ⁶³ University of Adelaide, Adelaide, SA 5005, Australia
- ⁶⁴ University of Birmingham, Birmingham, B15 2TT, United Kingdom

- ⁶⁵ *University of Florida, Gainesville, FL 32611, USA*
⁶⁶ *University of Glasgow, Glasgow, G12 8QQ, United Kingdom*
⁶⁷ *University of Maryland, College Park, MD 20742 USA*
⁶⁸ *University of Massachusetts - Amherst, Amherst, MA 01003, USA*
⁶⁹ *University of Michigan, Ann Arbor, MI 48109, USA*
⁷⁰ *University of Minnesota, Minneapolis, MN 55455, USA*
⁷¹ *University of Oregon, Eugene, OR 97403, USA*
⁷² *University of Rochester, Rochester, NY 14627, USA*
⁷³ *University of Salerno, I-84084 Fisciano (Salerno), Italy and INFN (Sezione di Napoli), Italy*
⁷⁴ *University of Sannio at Benevento, I-82100 Benevento, Italy and INFN (Sezione di Napoli), Italy*
⁷⁵ *University of Southampton, Southampton, SO17 1BJ, United Kingdom*
⁷⁶ *University of Strathclyde, Glasgow, G1 1XQ, United Kingdom*
⁷⁷ *University of Western Australia, Crawley, WA 6009, Australia*
⁷⁸ *University of Wisconsin-Milwaukee, Milwaukee, WI 53201, USA*
⁷⁹ *Washington State University, Pullman, WA 99164, USA and*
(Dated: September 13, 2011)

The gravitational-wave (GW) sky may include nearby pointlike sources as well as astrophysical and cosmological stochastic backgrounds. Since the relative strength and angular distribution of the many possible sources of GWs are not well constrained, searches for GW signals must be performed in a model-independent way. To that end we perform two directional searches for persistent GWs using data from the LIGO S5 science run: one optimized for pointlike sources and one for arbitrary extended sources. The latter result is the first of its kind. Finding no evidence to support the detection of GWs, we present 90% confidence level (CL) upper-limit maps of GW strain power with typical values between $2 - 20 \times 10^{-50} \text{ strain}^2 \text{ Hz}^{-1}$ and $5 - 35 \times 10^{-49} \text{ strain}^2 \text{ Hz}^{-1} \text{ sr}^{-1}$ for pointlike and extended sources respectively. The limits on pointlike sources constitute a factor of 30 improvement over the previous best limits. We also set 90% CL limits on the narrow-band root-mean-square GW strain from interesting targets including Sco X-1, SN1987A and the Galactic Center as low as $\approx 7 \times 10^{-25}$ in the most sensitive frequency range near 160 Hz. These limits are the most constraining to date and constitute a factor of 5 improvement over the previous best limits.

I. INTRODUCTION

One of the most ambitious goals of gravitational-wave (GW) astronomy is to measure the stochastic cosmological gravitational-wave background (CGB), which can arise through a variety of mechanisms including amplification of vacuum fluctuations following inflation [1], phase transitions in the early universe [2, 3], cosmic strings [4, 5] and pre-Big Bang models [6, 7]. The CGB may be masked by an astrophysical gravitational-wave background (AGB), interesting in its own right, which can arise from the superposition of unresolved sources such as core-collapse supernovae [8, 9], neutron-star excitations [10, 11], binary mergers [12, 13], persistent emission from neutron stars [14, 15] and compact objects around supermassive black holes [16, 17].

We present the results of two analyses using data from the LIGO S5 science run: a radiometer analysis optimized for pointlike sources and a spherical-harmonic decomposition analysis, which allows for arbitrary angular distributions. This work presents the first measurement of the GW sky in a framework consistent with an arbitrary extended source.

II. LIGO DETECTORS AND THE S5 SCIENCE RUN

We analyze data from LIGO's 4 km and 2 km detectors (H1 and H2) in Hanford, WA and the 4 km detector (L1) in Livingston Parish, LA during the S5 science run, which took place between Nov. 5, 2005 and Sep. 30, 2007. During S5, both H1 and L1 reached a strain sensitivity of $3 \times 10^{-23} \text{ strain Hz}^{-1/2}$ in the most sensitive region between 100 – 200 Hz [18] and collected 331 days of coincident H1L1 and H2L1 data. S5 saw milestones in GW astronomy including limits on the emission of GWs from the Crab pulsar that surpass those inferred from the Crab's spindown [19], as well as limits on the isotropic CGB that surpass indirect limits from Big Bang nucleosynthesis and the cosmic microwave background [20]. This work builds on [20, 21].

III. METHODOLOGY

Following [21, 22] we present a framework for analyzing the angular distribution of GWs. We assume that the GW signal is stationary and unpolarized, but not necessarily isotropic. It follows that the GW energy density $\Omega_{\text{GW}}(f)$, can be expressed in terms of the GW power

^aElectronic address: ethrane@physics.umn.edu

spectrum, $\mathcal{P}(f, \hat{\Omega})$:

$$\Omega_{\text{GW}}(f) \equiv \frac{f}{\rho_c} \frac{d\rho_{\text{GW}}}{df} = \frac{2\pi^2}{3H_0^2} f^3 \int_{S^2} d\hat{\Omega} \mathcal{P}(f, \hat{\Omega}). \quad (1)$$

Here f is frequency, $\hat{\Omega}$ is sky location, ρ_c is the critical density of the universe and H_0 is Hubble's constant. We further assume that $\mathcal{P}(f, \hat{\Omega})$ can be factored (in our analysis band) into an angular power spectrum, $\mathcal{P}(\hat{\Omega})$, and a spectral shape, $\bar{H}(f) \equiv (f/f_0)^\beta$, parameterized by the spectral index β and reference frequency f_0 . We set $f_0 = 100$ Hz to be in the sensitive range of the LIGO interferometers.

Our goal is to measure $\mathcal{P}(\hat{\Omega})$ for two power-law signal models. In the cosmological model, $\beta = -3$ ($\Omega_{\text{GW}}(f) = \text{const}$), which is predicted, e.g., for the amplification of vacuum fluctuations following inflation (see [23] and references therein). In the astrophysical model, $\beta = 0$ ($\bar{H}(f) = \text{const}$), which emphasizes the strain sensitivity of the LIGO detectors.

We estimate $\mathcal{P}(\hat{\Omega})$ two ways. The *radiometer algorithm* [21, 24, 25] assumes the signal is a point source characterized by a single direction $\hat{\Omega}_0$ and amplitude, $\eta(\hat{\Omega}_0)$:

$$\mathcal{P}(\hat{\Omega}) \equiv \eta(\hat{\Omega}_0) \delta^2(\hat{\Omega}, \hat{\Omega}_0). \quad (2)$$

It is applicable to a GW sky dominated by a limited number of widely separated point sources. As the number of point sources is increased, however, the interferometer beam pattern will cause the signals to interfere and partly cancel. Thus, radiometer maps do not apply to extended sources. Since pointlike signals are expected to arise from astrophysical sources, we use $\beta = 0$ for the radiometer analysis.

The *spherical-harmonic decomposition (SHD) algorithm* is used for both $\beta = -3$ (cosmological) and $\beta = 0$ (astrophysical) sources. It allows for the possibility of an extended source with an arbitrary angular distribution, characterized by spherical-harmonic coefficients \mathcal{P}_{lm} such that

$$\mathcal{P}(\hat{\Omega}) \equiv \sum_{lm} \mathcal{P}_{lm} Y_{lm}(\hat{\Omega}). \quad (3)$$

The series is cut off at l_{max} , allowing for angular scale $\sim 2\pi/l_{\text{max}}$. The flexibility of the spherical-harmonic algorithm comes at the price of somewhat diminished sensitivity to point sources, and thus the two algorithms are complementary.

We choose l_{max} so as to minimize the sky average of the product of $\sigma(\hat{\Omega})$ and \bar{A} , where $\sigma(\hat{\Omega})$ is the uncertainty associated with $\mathcal{P}(\hat{\Omega})$ and \bar{A} is the typical angular area of a resolved patch of sky [37]. Since $\bar{A} = 4\pi/N_{\text{indep}} \propto 1/(l_{\text{max}} + 1)^2$ (where N_{indep} is the number of independent parameters), this procedure amounts to choosing l_{max} to maximize the sensitivity obtained by integrating over the typical search aperture (angular resolution). We obtain $l_{\text{max}} = 7$ and 12 for $\beta = -3$ and $\beta = 0$, respectively.

Since the search aperture becomes smaller at the higher frequencies emphasized by $\beta = 0$, l_{max} is larger for $\beta = 0$ than for $\beta = -3$.

Both algorithms can be framed in terms of a “dirty map”, X_ν , which represents the signal convolved the Fisher matrix, $\Gamma_{\mu\nu}$:

$$X_\nu = \sum_{ft} \gamma_\nu^*(f, t) \frac{\bar{H}(f)}{P_1(f, t)P_2(f, t)} C(f, t) \quad (4)$$

$$\Gamma_{\mu\nu} = \sum_{ft} \gamma_\mu^*(f, t) \frac{\bar{H}^2(f)}{P_1(f, t)P_2(f, t)} \gamma_\nu(f, t). \quad (5)$$

Here both the Greek indices μ and ν take on values of lm for the SHD algorithm and $\hat{\Omega}$ for the radiometer algorithm, for which we use the pixel basis. The two bases are related using spherical-harmonic basis functions:

$$X_{\hat{\Omega}} = \sum_{lm} X_{lm} Y_{lm}(\hat{\Omega}). \quad (6)$$

$C(f, t)$, meanwhile, is the cross spectral density generated from the H1L1 or H2L1 pairs. $P_1(f, t)$ and $P_2(f, t)$ are the individual power spectral densities, and $\gamma_\mu(f, t)$ is the angular decomposition of the overlap reduction function $\gamma(\hat{\Omega}, f, t)$, which characterizes the orientations and frequency response of the detectors [22]:

$$\gamma_\mu(f, t) \equiv \int_{S^2} d\hat{\Omega} \gamma(\hat{\Omega}, f, t) \mathbf{e}_\mu(\hat{\Omega}) \quad (7)$$

$$\gamma(\hat{\Omega}, f, t) = \frac{1}{2} F_1^A(\hat{\Omega}, t) F_2^A(\hat{\Omega}, t) e^{i2\pi f \hat{\Omega} \cdot (\Delta \vec{x}_{12}(t))/c}. \quad (8)$$

Here $F_I^A(\hat{\Omega}, t)$ characterizes the detector response of detector I to a GW with polarization A , $\mathbf{e}_\mu(\hat{\Omega})$ is a basis function, c is the speed of light and $\Delta \vec{x}_{12} \equiv \vec{x}_1 - \vec{x}_2$ is the difference between the interferometer locations. A detailed discussion of these quantities can be found in [22].

In [22] it was shown that the maximum-likelihood estimators of GW power are given by $\hat{\mathcal{P}} = \Gamma^{-1} X$. The inversion of Γ is complicated by singular eigenvalues associated with modes to which the Hanford-Livingston (HL) detector network is insensitive. This singularity can be handled two ways. The radiometer algorithm assumes the signal is pointlike, implying that correlations between neighboring pixels can be ignored. Consequently, we can replace Γ^{-1} with $(\Gamma_{\hat{\Omega}\hat{\Omega}})^{-1}$ to estimate the point source amplitude $\eta(\hat{\Omega})$ (see Eq. 2). (We note that pointlike sources create signatures in our sky maps that typically span several degrees or more; see [21].)

The SHD algorithm, on the other hand, targets extended sources, so the full Fisher matrix must be taken into account. We regularize Γ by removing a fraction, \mathcal{F} , of the modes associated with the smallest eigenvalues, to which the HL network is relatively insensitive. \mathcal{F} is known as the regularization cutoff. By removing some modes from the Fisher matrix, we obtain a regularized inverse Fisher matrix, Γ_R^{-1} , thereby introducing a bias,

the implications of which are discussed below. For now, we note that the bias depends on the angular distribution of the signal.

We thereby obtain the estimators

$$\hat{\eta}_{\hat{\Omega}} = (\Gamma_{\hat{\Omega}\hat{\Omega}})^{-1} X_{\hat{\Omega}} \quad (9)$$

$$\hat{\mathcal{P}}_{lm} = \sum_{l'm'} (\Gamma_R^{-1})_{lm,l'm'} X_{l'm'}, \quad (10)$$

with uncertainties

$$\sigma_{\hat{\Omega}}^{\text{rad}} = (\Gamma_{\hat{\Omega}\hat{\Omega}})^{-1/2} \quad (11)$$

$$\sigma_{lm}^{\text{sph}} = [(\Gamma_R^{-1})_{lm,lm}]^{1/2}. \quad (12)$$

We refer to $\hat{\mathcal{P}}_{\hat{\Omega}} \equiv \sum_{lm} \hat{\mathcal{P}}_{lm} Y_{lm}(\hat{\Omega})$ as the “clean map” and $\hat{\eta}_{\hat{\Omega}}$ as the “radiometer map.” We note that $\hat{\eta}_{\hat{\Omega}}$ has units of $\text{strain}^2 \text{Hz}^{-1}$ whereas $\hat{\mathcal{P}}_{\hat{\Omega}}$ has units of $\text{strain}^2 \text{Hz}^{-1} \text{sr}^{-1}$.

In choosing \mathcal{F} one must balance the competing demands of reconstruction accuracy (sensitivity to the modes that are kept) with the bias associated with the modes that are removed. In practice, we do not know the bias associated with \mathcal{F} since it depends on the unknown signal distribution $\mathcal{P}(\hat{\Omega})$. Therefore, we choose a value of \mathcal{F} that tends to produce reliably reconstructed maps with minimal bias for simulated signals. Following [22], we use $\mathcal{F} = 1/3$, which was shown to be a robust regularization cutoff for simulated signals including maps characterized by one or more point sources, dipoles, monopoles and an extended source clustered in the galactic plane (see [22]).

In the case of the SHD algorithm, we construct an additional statistic (see [22]),

$$\hat{C}_l \equiv \frac{1}{2l+1} \sum_m [|\hat{\mathcal{P}}_{lm}|^2 - (\Gamma_R^{-1})_{lm,lm}], \quad (13)$$

which describes the angular scale of the clean map. The subtracted second term makes the estimator unbiased so that $\langle \hat{C}_l \rangle = 0$ when no signal is present. The expected noise distribution of \hat{C}_l is highly non-Gaussian for small values of l , and so the upper limits presented below are calculated numerically. The \hat{C}_l are analogous to similar quantities defined in the context of temperature fluctuations of the cosmic microwave background (see, e.g., [26]).

The analysis was performed using the S5 stochastic analysis pipeline. This pipeline has been tested with hardware and software injections, and the successful recovery of isotropic hardware injections is documented in [20]. The recovery of anisotropic software injections is demonstrated in [22]. We parse time series into 60s, Hann-windowed, 50%-overlapping segments, which are coarse-grained to achieve 0.25 Hz resolution. We apply a stationarity cut described in [21], which rejects $\sim 3\%$ of the cross-correlated segments. We also mask frequency bins associated with instrumental lines (e.g., harmonics of the 60 Hz mains power, calibration lines and suspension-wire resonances) as well as injected, simulated pulsar signals. For $\beta = -3, 0$ we include frequency

bins up to 200, 500 Hz, so that $\sigma(\hat{\Omega})$ is within $\lesssim 2\%$ of the minimum possible value. Thirty-three frequency bins are masked, corresponding to 2% of the frequency bins between 40 – 500 Hz used in the broadband analyses. For additional details about the S5 stochastic pipeline, see [20].

IV. SIGNIFICANCE AND UPPER LIMIT CALCULATIONS

In order to determine if there is a statistically significant GW signature, we are primarily interested in the significance of outliers—the highest signal-to-noise ratio (SNR) frequency bin or sky-map pixel. It is therefore necessary to calculate the expected noise probability distribution of the maximum SNR given many independent trials (when considering maximum SNR in a spectral band) and given many *dependent* trials (when considering maximum SNR for a sky map).

For N independent frequency bins, the probability density function, $\pi(\rho_{\text{max}})$, of maximum SNR, ρ_{max} , is given by

$$\pi(\rho_{\text{max}}) \propto \left[1 + \text{erf}\left(\rho_{\text{max}}/\sqrt{2}\right)\right]^{N-1} e^{-\rho_{\text{max}}^2/2}. \quad (14)$$

Here we have assumed that the stochastic point estimate is Gaussian distributed. The Gaussianity of $\hat{\mathcal{P}}_{\hat{\Omega}}$ and $\hat{\eta}_{\hat{\Omega}}$, calculated by summing over many $\mathcal{O}(500\text{K})$ independent segments, is expected to arise due to the central limit theorem [27]. Additionally, we find the Gaussian-noise hypothesis to be consistent with time-slide studies, wherein we perform the cross-correlation analysis with an unphysical time-shift in order to wash out astrophysical signals and thereby obtain different realizations of detector noise.

The distribution of maximum SNR for a sky map is more subtle due to the non-zero covariances that exist between different pixels (or patches) on the sky. For this case, we calculate $\pi(\rho_{\text{max}})$ numerically, by simulating many realizations of dirty maps that have expected covariances described by the Fisher matrix Γ . Figure 1 shows the numerically determined $\pi(\rho_{\text{max}})$ for the $\beta = -3$ clean map generated with Gaussian noise.

The likelihood function for $\mathcal{P}(\hat{\Omega})$ at each point in the sky can be described as a normal distribution with mean $\hat{\mathcal{P}}_{\hat{\Omega}}$ and a variance $(\sigma_{\hat{\Omega}}^{\text{sph}})^2$. In the case of the SHD algorithm, regularization introduces a signal-dependent bias. Without knowing the true distribution of $\mathcal{P}(\hat{\Omega})$, it is impossible to know the bias exactly, but it is possible to set a conservative upper limit by assuming that on average the modes removed through regularization contain no more GW power than the modes that are kept.

To implement this assumption, we calculate $\hat{\mathcal{P}}_{lm}$ with a regularization scheme that sets eigenvalues of removed modes to zero, whereas σ_{lm}^{sph} is conservatively calculated using a regularization scheme that sets eigenvalues of removed modes to the average eigenvalue of the kept

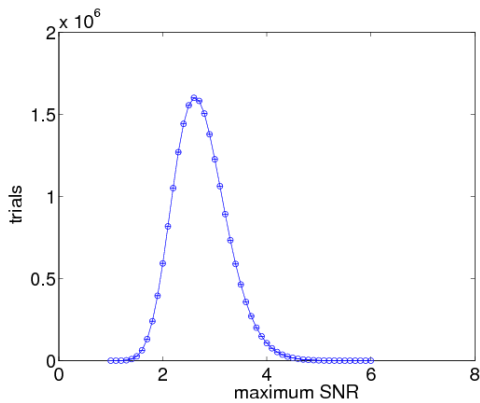


FIG. 1: Numerically calculated distribution of the maximum SNR for $\beta = -3$ clean maps created from Gaussian noise.

modes. This has the effect of widening the likelihood function at each sky location. The upper limits become on average 25% larger than they would be if we had calculated $\sigma_{lm}^{\text{sp}}h$ using the same regularization scheme as $\hat{\mathcal{P}}_{lm}$.

Following the same procedure as in [20], we marginalize over the H1, H2, and L1 calibration uncertainties, which were measured to be 10%, 10%, and 13%, respectively [28] [38]. The posterior distribution is obtained by multiplying the marginalized likelihood function by a prior, which we take to be flat above $\mathcal{P}(\hat{\Omega}) > 0$ [39]. The Bayesian upper limits are then determined by integrating the posterior out to the value of $\mathcal{P}(\hat{\Omega})$ which includes 90% of the total area under the distribution. The calculation of upper limits on $\eta_{\hat{\Omega}}$ is analogous except we need not take into account the effects of regularization.

V. RESULTS

Sky maps: Figure 2 presents sky map results for the different analyses: SHD algorithm with $\beta = -3$ (left), SHD with $\beta = 0$ (center), and radiometer with $\beta = 0$ (right). The top row contains SNR maps. The maximum SNR values are 3.1 (with significance $p = 25\%$), 3.1 (with $p = 56\%$), and 3.2 (with $p = 53\%$) respectively. These p -values take into account the number of search directions and covariances between different sky patches (see IV). Observing no evidence of GWs, we set upper limits on GW power as a function of direction. The 90% confidence level (CL) upper limit maps are given in the bottom row. For the SHD method with $\beta = -3$, the limits are between $5 - 31 \times 10^{-49} \text{ strain}^2 \text{ Hz}^{-1} \text{ sr}^{-1}$; for SHD with $\beta = 0$, the limits are between $6 - 35 \times 10^{-49} \text{ strain}^2 \text{ Hz}^{-1} \text{ sr}^{-1}$; and for the radiometer with $\beta = 0$, the limits are between $2 - 20 \times 10^{-50} \text{ strain}^2 \text{ Hz}^{-1}$.

The strain power limits can also be expressed in terms

of the GW energy flux per unit frequency [21]:

$$\hat{F}(f, \hat{\Omega}) = \frac{c^3 \pi f_0^2}{4G} \left(\frac{f}{f_0} \right)^{\beta+2} \hat{\mathcal{P}}_{\hat{\Omega}} \quad (15)$$

$$= \left(3.18 \times 10^{42} \frac{\text{erg}}{\text{cm}^2 \text{ s}} \right) \left(\frac{f}{100 \text{ Hz}} \right)^{\beta+2} \hat{\mathcal{P}}_{\hat{\Omega}}. \quad (16)$$

(Radiometer energy flux is obtained by replacing $\hat{\mathcal{P}}_{\hat{\Omega}}$ with $\hat{\eta}_{\hat{\Omega}}$.) The corresponding values are $2 - 10 \times 10^{-6} (f/100 \text{ Hz})^{-1} \text{ erg cm}^{-2} \text{ s}^{-1} \text{ Hz}^{-1} \text{ sr}^{-1}$ and $2 - 11 \times 10^{-6} (f/100 \text{ Hz})^2 \text{ erg cm}^{-2} \text{ s}^{-1} \text{ Hz}^{-1} \text{ sr}^{-1}$ for the SHD method, and $6 - 60 \times 10^{-8} (f/100 \text{ Hz})^2 \text{ erg cm}^{-2} \text{ s}^{-1} \text{ Hz}^{-1}$ for the radiometer. The radiometer map constitutes a factor of ~ 30 improvement over the previous best strain power limits [21].

When comparing the SHD analysis with $\beta = 0$ and the radiometer upper limits obtained using the same spectrum, it is important to note that these maps have different units. The radiometer map has units of $\text{strain}^2 \text{ Hz}^{-1}$ because the radiometer analysis effectively integrates the power from a GW point source over solid angle. The SHD maps, on the other hand, have units of $\text{strain}^2 \text{ Hz}^{-1} \text{ sr}^{-1}$. If we scale the SHD limit maps by the typical diffraction limited resolution ($\bar{A} \approx 0.1 \text{ sr}$), then the limits are more comparable. The radiometer algorithm limits are lower (by a factor of $\lesssim 2$) because it requires a stronger assumption about the signal model (a single point source), whereas the SHD algorithm is model-independent.

Figure 3 show 90% CL upper limits on the C_l . Since the \mathcal{P}_{lm} have units of strain power ($\text{strain}^2 \text{ Hz}^{-1} \text{ sr}^{-1}$), the C_l have the somewhat unusual units of $\text{strain}^4 \text{ Hz}^{-2} \text{ sr}^{-2}$.

Targeted searches: Sco X-1 is a nearby (2.8 kpc) low-mass X-ray binary likely to include a neutron star spun up through accretion. Its spin frequency is unknown. It has been suggested that this accretion torque is balanced by GW emission [29]. The Doppler line broadening due to the orbital motion is smaller than the chosen $\delta f = 0.25 \text{ Hz}$ bin width for frequencies below $\approx 930 \text{ Hz}$ [30]. At higher frequencies, the signal is certain to span two bins. We determine the maximum value of SNR in the direction of Sco X-1 to be 3.6 at $f = 1770.50 \text{ Hz}$, which has a significance of $p = 73\%$ given the $\mathcal{O}(7000)$ independent frequency bins. Thus in Fig. 4 (first panel) we present limits on root-mean-square (RMS) strain, $h_{\text{RMS}}(f, \hat{\Omega})$, as a function of frequency in the direction of Sco X-1 (RA, dec) = (16.3 hr, 15.6°). These limits improve on the previous best limits by a factor of ~ 5 [21]. RMS strain is related to narrow-band GW power via

$$h_{\text{RMS}}(f, \hat{\Omega}) = \left[\eta(f, \hat{\Omega}) \delta f \right]^{1/2}, \quad (17)$$

and is better suited for comparison with searches for periodic GWs, which typically constrain the peak strain amplitude, h_0 , marginalized over neutron star parameters ι and ψ (see, e.g., [31]). Our limits on h_{RMS} are for a circularly polarized signal from a pulsar whose spin axis is aligned with the line of sight. Marginalizing over

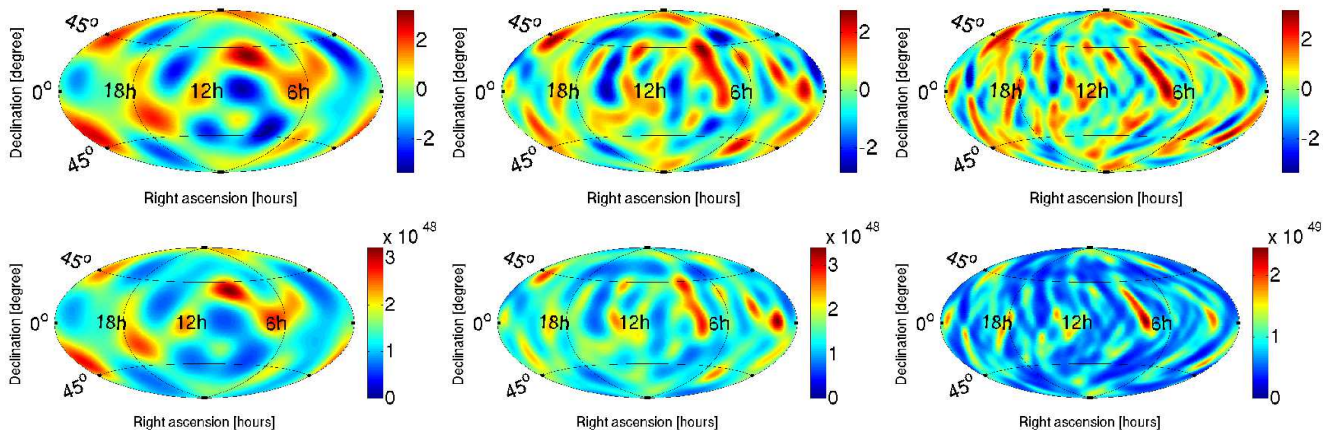


FIG. 2: Top row: Signal-to-noise ratio maps for the three different analyses described in this paper: SHD clean map for $\beta = -3$ (left), SHD clean map for $\beta = 0$ (center), and radiometer for $\beta = 0$ (right). All three SNR maps are consistent with detector noise. The p-values associated with each map's maximum SNR are (from left to right) $p = 25\%$, $p = 56\%$, $p = 53\%$. Bottom row: The corresponding 90% CL upper limit maps on strain power in units of $\text{strain}^2\text{Hz}^{-1}\text{sr}^{-1}$ for the SHD algorithm, and units of $\text{strain}^2\text{Hz}^{-1}$ for the radiometer algorithm.

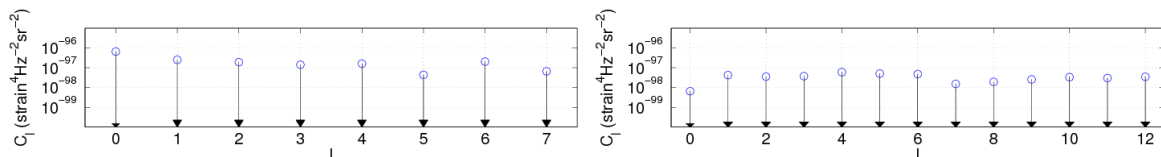


FIG. 3: Upper limits on C_l at 90% CL vs l for the SHD analyses for $\beta = -3$ (left) and $\beta = 0$ (right). The \hat{C}_l are consistent with detector noise.

ι and ψ and converting from RMS to peak amplitude causes the limits to change by a sky-dependent factor of ≈ 2.3 [32]. We note that these limits are on the RMS strain in each bin as opposed to the total RMS strain from Sco X-1, which might span as many as two bins. The frequency axis refers to the observed GW frequency as opposed to the intrinsic GW frequency.

We also look for statistically significant outliers associated with the Galactic Center (RA, dec) = (17.8 hr, -29°) and SN1987A (RA, dec) = (5.6 hr, -69°). The maximum SNR values are 3.5 at $f = 203.25$ Hz with $p = 85\%$ and 4.3 at 1367.25 Hz with $p = 7\%$, respectively. Limits on RMS strain are given in the right panel of Fig. 4.

VI. CONCLUSIONS

We performed two directional analyses for persistent GWs: the radiometer analysis, which is optimized for point sources, and the complementary spherical-harmonic decomposition (SHD) algorithm, which allows for arbitrary extended sources. Neither analysis finds evidence of GWs. Thus we present upper-limit maps of GW power and also limits on the RMS strain from Sco X-1, the Galactic Center and SN1987A. The radiometer map limits improve on the previous best limits [21] by a fac-

tor of 30 in strain power, and limits on RMS strain from Sco X-1 constitute a factor of 5 improvement in strain over the previous best limits [21]. The SHD clean maps represent the first effort to look for anisotropic extended sources of GWs.

With the ongoing construction of second-generation GW interferometers, we are poised to enter a new era in GW astronomy. Advanced detectors [33–36] are expected to achieve strain sensitivities approximately 10 times lower than initial LIGO, and advances in seismic isolation are expected to extend the frequency band down from 40 Hz to 10 Hz [33]. By adding additional detectors to our network, we expect to reduce degeneracies in the Fisher matrix and improve angular resolution. These improvements will allow advanced detector networks to probe plausible models of astrophysical stochastic foregrounds and some cosmological models such as cosmic strings.

Acknowledgments

The authors gratefully acknowledge the support of the United States National Science Foundation for the construction and operation of the LIGO Laboratory, the Science and Technology Facilities Council of the United Kingdom, the Max-Planck-Society, and the State

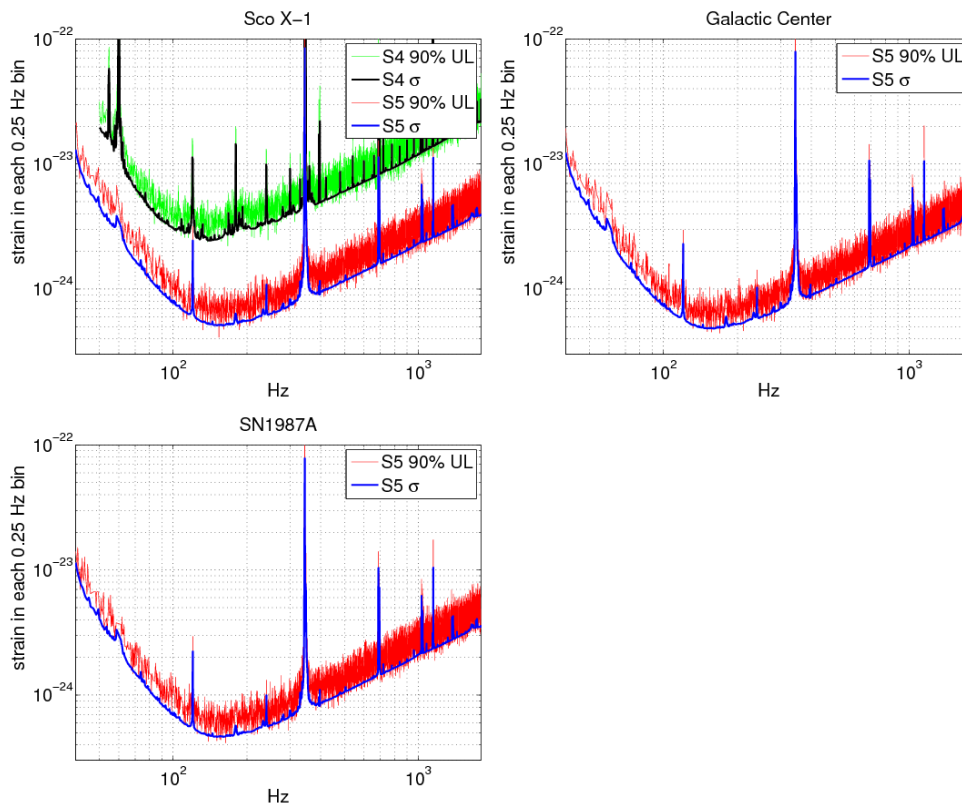


FIG. 4: Radiometer 90% upper limits on RMS strain in each 0.25 Hz wide bin as a function of frequency for Sco X-1 (top-left), the Galactic Center (top-right) and SN1987A (bottom). The large spikes correspond to harmonics of the 60 Hz power mains, calibration lines and suspension-wire resonances. The previous S4 upper limits for Sco X-1 [21] are also plotted in the top-left panel, illustrating the improvement in the upper limits obtained by using the LIGO S5 data. This is the first radiometer measurement of the Galactic Center and SN1987A.

of Niedersachsen/Germany for support of the construction and operation of the GEO600 detector, and the Italian Istituto Nazionale di Fisica Nucleare and the French Centre National de la Recherche Scientifique for the construction and operation of the Virgo detector. The authors also gratefully acknowledge the support of the research by these agencies and by the Australian Research Council, the International Science Linkages program of the Commonwealth of Australia, the Council of Scientific and Industrial Research of India, the Istituto Nazionale di Fisica Nucleare of Italy, the Spanish Ministerio de Educación y Ciencia, the Conselleria d'Economia Hisenda

i Innovació of the Govern de les Illes Balears, the Foundation for Fundamental Research on Matter supported by the Netherlands Organisation for Scientific Research, the Polish Ministry of Science and Higher Education, the FOCUS Programme of Foundation for Polish Science, the Royal Society, the Scottish Funding Council, the Scottish Universities Physics Alliance, The National Aeronautics and Space Administration, the Carnegie Trust, the Leverhulme Trust, the David and Lucile Packard Foundation, the Research Corporation, and the Alfred P. Sloan Foundation. This is LIGO document #P1000031.

-
- [1] E. W. Kolb and M. S. Turner, *The Early Universe* (Westview Press, 1994).
- [2] A. A. Starobinski, *JETP Lett.* **30** (1979).
- [3] R. Bar-Kana, *Phys. Rev. D* **50** (1994).
- [4] T. W. B. Kibble, *J. Phys.* **A9** (1976).
- [5] T. Damour and A. Vilenkin, *Phys. Rev. D* **71** (2005).
- [6] A. Buonanno, *Phys. Rev. D* **55** (1997).
- [7] V. Mandic and A. Buonanno, *Phys. Rev. D* **73** (2006).
- [8] E. Howell et al., *Mon. Not. R. Ast. Soc.* **351**, 1237 (2004).
- [9] V. Ferrari, S. Matarrese, and R. Schneider, *Mon. Not. R. Ast. Soc.* **303**, 258 (1999).
- [10] V. Ferrari, S. Matarrese, and R. Schneider, *Mon. Not. R. Ast. Soc.* **303**, 258 (1999).
- [11] G. Sigl, *J. Cosmol. Astropart. Phys.* **JCAP04**, 002 (2006).
- [12] T. Regimbau and B. Chauvineaux, *Class. Quantum Grav.* **24**, 627 (2007).
- [13] A. J. Farmer and E. S. Phinney, *Mon. Not. R. Ast. Soc.* **346**, 1197 (2003).
- [14] T. Regimbau and J. A. de Freitas Pacheco, *Astron. As-*

- trophys. **376**, 381 (2001).
- [15] T. Regimbau and J. A. de Freitas Pacheco, *Astron. Astrophys.* **447**, 1 (2006).
- [16] L. Barack and C. Cutler, *Phys. Rev. D* **70**, 122002 (2004).
- [17] G. Sigl, J. Schnittman, and A. Buonanno, *Phys. Rev. D* **75**, 024034 (2007).
- [18] B. P. Abbott et al., *Rep. Prog. Phys.* **72**, 076901 (2009).
- [19] B. Abbott et al., *Astrophys. J. Lett.* **683**, 45 (2008).
- [20] B. Abbott et al., *Nature* **460**, 990 (2009).
- [21] B. Abbott et al., *Phys. Rev. D* **76**, 082003 (2007), [astro-ph/0703234](#).
- [22] E. Thrane et al., *Phys. Rev. D* **80**, 122002 (2009).
- [23] M. Maggiore, *Phys. Rept.* **331**, 283 (2000).
- [24] S. W. Ballmer, *Class. Quantum Grav.* **23**, S179 (2006).
- [25] S. Mitra, S. Dhurandhar, T. Souradeep, et al., *Phys. Rev. D* **77**, 042002 (2008).
- [26] G. Hinshaw et al., *Astrophys. J. Suppl.* **180**, 225 (2009).
- [27] B. Allen and J. D. Romano, *Phys. Rev. D* **59**, 102001 (1999).
- [28] J. Abadie et al., *Nucl. Instrum. Meth. A* **624**, 223 (2010).
- [29] D. Chakrabarty et al., *Nature* **424**, 42 (2003).
- [30] D. Steeghs and J. Casares, *Astrophys. J.* **568**, 273 (2002).
- [31] B. Abbott et al., *Phys. Rev. D* **76**, 082001 (2007).
- [32] C. Messenger, *Understanding the sensitivity of the stochastic radiometer analysis in terms of the strain tensor amplitude*, LIGO Document T1000195-v1 (2010).
- [33] G. Harry for the LIGO Science Collaboration, *Class. Quantum Grav.* **27**, 084006 (2010).
- [34] J R Smith for the LIGO Science Collaboration, *Class. Quantum Grav.* **26**, 114013 (2009).
- [35] F. Acernese for The Virgo Collaboration, *Class. Quantum Grav.* **23**, S63 (2006).
- [36] K Kuroda for the LCGT Collaboration, *Class. Quantum Grav.* **27**, 084004 (2010).
- [37] The data were first processed with $l_{\max} = 20$; the present method of choosing l_{\max} was then adopted a posteriori in order to more accurately model the angular resolution of the interferometer network.
- [38] We follow the marginalization scheme used in [20], but note that this does not take into account covariance between baselines with a shared detector. Because the H2L1 baseline only contributes about 10% of the sensitivity, and the calibration uncertainty is on the order of 10% to start with, this effect is only on the order of 1%. Work is ongoing to take this effect into account, which we expect to be more important for baselines with comparable sensitivities.
- [39] A prior constructed from [21] would be nearly flat anyway since the strain sensitivity has improved ten-fold since the S4 science run.